Drug-target binding quantitatively predicts optimal antibiotic dose levels

Fabrizio Clarelli[1], Adam Palmer[2], Bhupender Singh[1], Merete Storflor[1], Silje Lauksund[1], Ted Cohen[3], Sören Abel[1,4,#], Pia Abel zur Wiesch[1,3,#,]* [ORCID: https://orcid.org/0000-0001-9420-9005]

1. Department of Pharmacy, Faculty of Health Sciences, University of Tromsø, Tromsø, Norway.
2. Laboratory of Systems Pharmacology, Harvard Medical School, Boston, MA, USA.
3. Department of Epidemiology of Microbial Diseases, Yale School of Public Health, New Haven, Connecticut, United States of America.
4. Centre for Molecular Medicine Norway, Nordic EMBL Partnership, Oslo, Norway.

\# Authors contributed equally

* e-mail: pia.z.wiesch@uit.no

Abstract

Combatting antibiotic resistance will require both new antibiotics and strategies to preserve the effectiveness of existing drugs. Both approaches would benefit from predicting optimal dosing of antibiotics based on drug-target binding parameters that can be measured early in drug development and that can change when bacteria become resistant. This would avoid the currently frequently employed trial-and-error approaches and might reduce the number of antibiotic candidates that fail late in drug development.

Here, we describe a computational model (COMBAT- COmputational Model of Bacterial Antibiotic Target-binding) that leverages accessible biochemical parameters to quantitatively predict antibiotic dose-response relationships. We validate our model with MICs of a range of quinolone antibiotics in clinical isolates demonstrating that antibiotic efficacy can be predicted from drug-target binding ($R^2 > 0.9$). To further challenge our approach, we do not only predict antibiotic efficacy from biochemical parameters, but also do the reverse: estimate the magnitude of changes in drug-target binding based on antibiotic dose-response curves. We experimentally demonstrate that changes in drug-target binding can be predicted from antibiotic dose-response curves with 92-94 % accuracy by exposing bacteria overexpressing target molecules to ciprofloxacin. To test the generality of COMBAT, we apply it to a different antibiotic class, the beta-lactam ampicillin, and can again predict binding parameters from dose-response curves with 90 % accuracy. We then apply COMBAT to predict antibiotic concentrations that can select for resistance due to novel resistance mutations.

Our goal here is dual: First, we address a fundamental biological question and demonstrate that drug-target binding determines bacterial response to antibiotics, although antibiotic action involves many additional effects downstream of drug-target binding. Second, we create a tool that can help accelerate drug development by predicting optimal dosing and preserve the efficacy of existing antibiotics by predicting optimal treatment for possible resistant mutants.

Introduction

The rise of antibiotic resistance represents an urgent public health threat. In order to effectively combat the spread of antibiotic resistance, we must optimize the use of existing drugs and develop new drugs that are effective against drug-resistant strains. Accordingly, methods to improve antibiotic dose levels to i) maximize efficacy against susceptible strains and ii) minimize resistance evolution play a key role in our defense against antibiotic resistant pathogens.

It is noteworthy that dosing strategies for treatment of susceptible strains (e.g., dosing level[1], dosing frequency[2], and treatment duration[3-5]) have recently been substantially improved, even for antibiotic treatments that have been standard of care for decades. This suggests that there likely remains significant room for optimization in our antibiotic treatment regimens. It also highlights the difficulty in identifying optimal dosing levels for new antibiotics. Indeed, optimizing dosing is one of the biggest challenges in drug development. Typically, time-consuming trial-and-error approaches are used and each failed drug candidate makes this process more expensive[6].

60 It is even more challenging to optimize dose levels to minimize the emergence of antibiotic
61 resistance, both for existing and novel antibiotics. There remains substantial debate about which
62 dosing strategies best prevent the emergence of resistant mutants during treatment[7-9]. In this
63 context, a useful concept that links antibiotic concentrations with resistance evolution is the
64 resistance selection window (mutant selection window) that ranges from the lowest
65 concentration at which the resistant strain grows faster than the wild-type, usually well below the
66 wild-type minimum inhibitory concentration (MIC), to the MIC of the resistant strain[10-12].
67 Antibiotic concentrations above the resistance selection window safeguard against *de novo*
68 resistance emergence. Antibiotic concentrations below the resistance selection window do not
69 kill the susceptible strain, but also do not favor the resistant strain and therefore do not promote
70 emergence of resistance. The latter may be preferable if one cannot dose above the MIC of the
71 resistant strain due to toxicity or solubility limits. To limit resistance emergence, it is therefore
72 important to identify the resistance selection window and optimize dosing accordingly.
73
74 Limitations in our knowledge of how antibiotic treatment regimens affect bacterial populations
75 contribute to the need for lengthy and expensive trial-and-error approaches, with the sheer
76 number of possible dosing regimens making it difficult to identify an optimal regimen. We argue
77 that this knowledge gap is a major limitation for the improvement of dosing regimens of existing
78 drugs and a real obstacle for the development of new antibiotics[13, 14].
79
80 Pharmacodynamic models that can make predictions of bacterial killing and selection on the
81 basis of drug-target interactions offer new promise to inform rational antibiotic dosing
82 practices[15]. Recently described models that include drug-target binding have been useful in

83 gaining a better qualitative understanding of complicated drug effects, such as post-antibiotic
84 effects, inoculum effects, and bacterial persistence[15-18]. However, to speed the development
85 of new antibiotics or to inform practices which minimize resistance, we require quantitative
86 predictions for antibiotics or resistant bacterial strains that do not exist yet. Models which permit
87 quantitative predictions of changes in drug efficacy as a function of modification of antibiotic
88 molecules (i.e. new drugs) or novel resistance mutations would be invaluable. Such tools would
89 advance our general mechanistic understanding of antibiotic action, could guide dosing trials of
90 new drugs, and suggest better dosing of existing drugs.
91
92 In this report, we describe a mechanistic computational modeling framework (COMBAT-
93 COmputational Model of Bacterial Antibiotic Target-binding) that allows us to predict drug
94 effects based solely on accessible biochemical parameters describing drug-target interaction.
95 These parameters can be determined early in drug development. We use this framework to
96 investigate how changes in drug target binding, either due to improvements in existing
97 antibiotics or due to resistance mutations in bacteria, affect antibiotic efficacy. We first show that
98 COMBAT accurately predicts bacterial susceptibility as a function of drug-target binding and,
99 conversely, allows inference of these biochemical parameters on the basis of observed patterns of
100 bacterial growth suppression or killing. We then use COMBAT to predict the susceptibility of
101 newly arising resistant variants based on the molecular mechanism of resistance and determine
102 the resistance selection window.
103
104 **Results**
105 **Quinolone target affinities correlate with antibiotic efficacy**

106 To investigate how biochemical changes in antibiotic action modifies bacterial susceptibility, we
107 explored how the affinity of antibiotics to their target affects the MIC. We compared the MICs of
108 quinolones, an antibiotic class in which individual antibiotics have a wide range of affinities to
109 their target, gyrase ($K_D \sim 10^{-4}$ - 10^{-7} M) but are of similar molecular sizes and have a similar mode
110 of action[19]. This choice allowed us to isolate the effects of differences in drug-target affinity
111 on the MIC.
112
113 We obtained binding affinities of quinolones to their gyrase target in *Escherichia coli* from
114 previous studies[20-24]. We then retrieved MIC data for several quinolones from clinical
115 Enterobacteriaceae isolates collected before 1990[25], i.e., before the widespread emergence of
116 quinolone resistance[19]. We assume that quinolone affinities obtained from clinical
117 Enterobacteriaceae isolates collected before the emergence of resistance correspond to those
118 measured in wild-type *E. coli*.
119
120 To make qualitative predictions of MICs, we employed a simplified model based on the
121 assumptions that i) drug-target binding occurs much more quickly than bacterial replication, ii)
122 the antibiotic concentration remains constant and iii) that during the 18 hours of an MIC assay,
123 the concentration gradient of the drug inside and outside the cell has equilibrated. Under these
124 assumptions, the MIC can be expressed as
125 $$MIC = K_D \frac{f_c}{1-f_c} \quad (1)$$
126
127 where K_D represents the affinity constant and f_c the fraction of the target bound at the MIC[26].
128 Accordingly, this model predicts that the MIC is linearly correlated with K_D.

129

130 Fig. 1 shows the correlations between drug-target affinities and MICs for seven quinolones and
131 clinical isolates of 11 different Enterobacteriaceae species. We observed a significant ($p < 0.018$)
132 linear correlation between MIC and K_D in all species, confirming the qualitative model
133 prediction.

134

135 **A quantitative model to predict antibiotic efficacy**

136 While it was encouraging that our model can qualitatively predict MIC changes, our aim was to
137 quantitatively predict antibiotic treatment performance. The simplified model assumes that the
138 binding kinetics are much faster than bacterial replication, which may not be true in all cases. To
139 expand the generalizability of the model, we extended the modeling framework to allow that
140 bacterial replication may occur in a similar time frame as drug-target binding events.

141

142 The full model (COMBAT- COmputational Model of Bacterial Antibiotic Target-binding)
143 describes the binding and unbinding of antibiotics to their targets and predicts how such binding
144 dynamics affects bacterial replication and death (Fig. 2a). In previous work linking drug-target
145 binding kinetics with bacterial replication[18], we described a population of bacteria with θ
146 target molecules per cell with a system of $\theta + 1$ (bacteria with 0, 1, …, θ bound target
147 molecules) ordinary differential equations (ODEs). This system increases in complexity with the
148 number of target molecules and makes fitting the model to data computationally too demanding
149 for most settings. To simplify this prior approach, we developed new mathematical models based
150 on partial differential equations (PDEs), where a single equation describes all bacteria
151 simultaneously. The sum of bacteria within all target occupancy states over time can be

described by a time kill curve (Fig. 2b), during which the bacterial population is characterized by the distribution of bacterial cells with different levels of target occupancies at each time-step (Fig. 2c). This curve can be visualized as a two-dimensional surface in a three-dimensional coordinate system where the number of bacteria is represented on the z-axis, the percent of bacteria with the fraction of bound target molecules on the x-axis, and time on the y-axis (Fig. 2d).

Antibiotic action is described by rates of binding (k_f) and unbinding (k_r) to bacterial target molecules (Fig. 2a, e). The binding of an antibiotic to a target results in the formation of an antibiotic-target molecule complex x, where x ranges between 0 and θ.

COMBAT consists of two mass balance equations: equation 2 describing bacterial numbers as a function of bound targets and time and equation 3 describing antibiotic concentration as a function of time (Methods section).

$$\frac{\partial B(x,t)}{\partial t} + \overbrace{\frac{\partial}{\partial x}(v_B(x,t)B(x,t))}^{Binding\ kinetics} = \overbrace{-r(x)B(x,t)F_{lim}(t) + S_B(x,t)F_{lim}(t)}^{Replication\ and\ its\ effects\ on\ binding} - \overbrace{\delta(x)B(x,t)}^{Death} \quad (2)$$

The term for binding kinetics is given in brown, the term for replication in blue and the term for death in red.

$$\frac{dA(t)}{dt} = -\hat{k}_f A(t) \int_0^\theta (\theta - x)B(x,t)dx + k_r \int_0^\theta xB(x,t)dx \quad (3)$$

where $v_B = v_f - v_r$, $v_f = \hat{k}_f A(t)(\theta - x)$ and $v_r = k_r x$. v_B, v_f, and v_r can be seen as a generalized velocity $v = \frac{dx}{dt}$.

174 Equation 4 (part of the replication term in equation 2) describes how daughter cells inherit bound
175 target molecules from the mother cell during replication:

176 $$S_B(x,t) = 2\int_x^\theta h(x,z)r(z)B(z,t)dz\,;\ \forall x \in [0,\theta] \quad (4)$$

177

178 Equation 5 (part of the replication term in equation 2) is a logistic growth model describing
179 reduced bacterial replication as the carrying capacity is approached:

180 $$F_{lim} = \left(1 - \frac{\int_0^\theta B(x,t)dx}{K}\right) \quad (5)$$

181

182 **Model fit to ciprofloxacin time-kill data**

183 We used the quinolone ciprofloxacin to quantitatively fit bacterial time-kill curves, since this is a
184 commonly used antibiotic for which binding parameters have been directly measured.
185 Supplementary Tab. S1 gives an overview of the known parameters used for fitting;
186 Supplementary Tab. S2 gives the parameters resulting from our fit.

187

188 The functional relationship between the levels of bacterial replication and death on the fraction
189 of bound target molecules is extremely hard to obtain experimentally. We therefore treated the
190 relationships between the fraction of bound target and bacterial replication and death as free
191 parameters in our model fitting. Ciprofloxacin is considered to have both bacteriostatic and
192 bactericidal action (mixed action)[27, 28], and we fitted functions for a monotonically decreasing
193 replication and a monotonically increasing killing with each successively bound target molecule
194 (see Methods & Supplementary Fig. S1).

195

196 Overall, we found that COMBAT could fit the time-kill curves well ($R^2 = 0.93$, Fig. 3a). Fig. 3b
197 shows the predicted bacterial replication $r(x)$ and death as a function of target occupancy $\delta(x)$
198 based on the fit obtained in Fig. 3a. After model calibration, we simulated bacterial replication
199 during exposure to different antibiotic concentrations for 18 h. For this simulation, positive
200 values indicate an increase in the number of bacteria, and negative values indicate a decrease in
201 the number of bacteria. We estimated a MIC of 0.0139 mg/L (Fig. 3c), a value that is within the
202 range of MIC determinations for wt *E. coli* (0.01 mg/L, 0.015 mg/L, 0.017 mg/L and 0.023 mg/L
203 [11, 29-31]).

204 **Accurate prediction of target overexpression from time-kill data**

205 Having shown that COMBAT can quantitatively fit experimental data on antibiotic action within
206 biologically plausible parameters, we continued to test the predictive ability of the model. Given
207 our hypothesis that modifications in antibiotic-target interactions lead to predictable changes in
208 bacterial susceptibility, we experimentally induced changes in the antibiotic-target interaction of
209 ciprofloxacin in *E. coli*. We then quantified these biochemical changes by fitting COMBAT to
210 corresponding time-kill curves and compared them to the experimental results. Ciprofloxacin
211 acts on gyrase A_2B_2 tetramers[19]. We used an *E. coli* strain for which both gyrase A and gyrase
212 B are under the control of a single inducible promoter (P_{lacZ}), such that the amount of gyrase
213 A_2B_2 tetramer can be experimentally manipulated[32]. We measured net growth rates for this
214 strain at different ciprofloxacin concentrations in the presence of 10 μM isopropyl β-D-1-
215 thiogalactopyranoside (IPTG; mild overexpression) and 100 μM IPTG (strong overexpression)
216 and compared it to the wild-type in the absence of the inducer (Fig. 4a).
217

218 Like previously reported, we find that increasing gyrase content makes *E. coli* more susceptible
219 to ciprofloxacin[32]. We fitted net growth rates allowing the target molecule content, i.e. gyrase
220 A_2B_2, to vary. We assumed that the only change between the different conditions was the amount
221 of target. We further assumed that the relationship between bound target and bacterial replication
222 or death did not differ between the control strain containing a mock plasmid (no IPTG) and the
223 experiments with overexpression (Fig. 4b, between 0 % and 100 %). Finally, we assumed that
224 the maximal kill rate at very high antibiotic concentrations was accurately measured in our
225 experiments and forced the function describing bacterial death through the measured value when
226 all target molecules are bound. We found the best fit for a 1.31x increase in $GyrA_2B_2$ target
227 molecule content for bacteria grown in the presence of 10 μM IPTG and a 2.02x increase in
228 $GyrA_2B_2$ target molecule content for those grown in the presence of 100 μM IPTG.
229
230 We subsequently tested these predictions experimentally by analyzing Gyrase A and B content
231 by western blot Fig. 4c; Supplementary Fig. S2). Using realistic association and dissociation
232 rates for biological complexes[33], we predicted a range of functional tetramers based on the
233 relative amount of Gyrase A and B proteins (Fig. 4d). Supplementary Tab. S3 details the
234 individual measurements, and the procedure to estimate tetramers is provided in the methods
235 section. We found that the observed overexpression was very close to our theoretical prediction,
236 with 1.43x [95 % CI 1.19-1.81] overexpression (model prediction = 1.31x overexpression) in the
237 presence of 10 μM IPTG and 2.15x [95 % CI 1.73-2.87] overexpression in the presence of
238 100 μM IPTG (model prediction = 2.02x overexpression).
239
240 **Accurate prediction of target occupancy at MIC from time-kill data**

241 Next, we tested whether COMBAT can be applied to the action of the beta-lactam ampicillin, a
242 very different antibiotic with a distinct mode of action from quinolones. Using published
243 pharmacodynamic data of *E. coli* exposed to ampicillin[31] also allowed us to compare
244 COMBAT predictions to established pharmacodynamic approaches. Most of the biochemical
245 parameters for ampicillin binding to its target, penicillin-binding proteins (PBPs), have been
246 determined experimentally (Supplementary Tab. S1). Ampicillin is believed to act as a
247 bactericidal drug[34], and this mode of action is supported by findings from single-cell
248 microscopy[26]. We therefore assume that ampicillin binding does not affect bacterial
249 replication. In order to model the consumption of beta-lactams at target inhibition and eventual
250 target recovery, we made small adjustments to equation 13 (see Methods, description of beta-
251 lactam action).
252
253 We fitted COMBAT to published time-kill curves of *E. coli* exposed to ampicillin (Fig. 5a).
254 Again, COMBAT provides a good fit to the experimental data between 0 min and 40-60 min.
255 After that time, observed bacterial killing showed a characteristic slowdown at high ampicillin
256 concentrations which is often attributed to persistence[18] (Fig. 5a). For the sake of simplicity,
257 we chose to omit bacterial population heterogeneity in this work and therefore cannot describe
258 persistence, even though COMBAT can be adapted to capture this phenomenon[18]. Because
259 ampicillin acts in an entirely bactericidal manner, we assume a constant replication rate (see
260 Methods & Supplementary Fig. S1) and fitted bacterial death as a function of target binding,
261 $\delta(x)$ (Fig. 5b, fitted parameters in Tab. S4). Fig. 5c shows the predicted net growth rate over a
262 range of drug concentrations. We estimated a MIC of 2.6 mg/L. This MIC is based on the
263 Clinical & Laboratory Standards Institute definition of the MIC determined at 18 h. The original

264 source of the MIC, which was based on experimental data and a pharmacodynamic model[31]
265 determined an MIC of 3.4 mg/L at 1 h. If we change our prediction to 1 h, our estimated MIC is
266 3.32 mg/L, which is within 2.5 % of the reported value[31].
267
268 Having established that COMBAT can also adequately capture the pharmacodynamics of
269 ampicillin, we next tested whether we can estimate experimentally determined target occupancy
270 at the MIC. Our estimated mean occupancy considering both living and dead bacteria is 89 %
271 (Fig. 5b), a value within previously reported experimental estimates from *Staphylococcus aureus*
272 (84-99 %)[35].
273
274 **Sensitivity of antibiotic efficacy to parameters of drug-target binding**
275 It is possible to vary all parameters in COMBAT and explore their effect. We used this to test
276 how hypothetical chemical changes to ampicillin or ciprofloxacin would affect antibiotic
277 efficacy (Supplementary Fig. S3-S11). These changes could reflect either bacterial resistance
278 mutations or modifications of the antibiotics themselves. We predict that changes in drug-target
279 affinity, K_D, have more profound effects than changes in target molecule content, bacterial
280 reaction to increasingly bound target (i.e. $\delta(x)$ and $r(x)$), or changes in target molecule content.
281 We also predict that the individual binding rates k_r and k_f, and not just the ratio of these terms,
282 the K_D, are important factors in efficiency. The faster a drug binds, the more efficient we
283 predicted it will be. One intuitive explanation for the observation that k_f drives efficacy is that a
284 slow binding fails to rapidly interfere with bacterial replication, which may allow for the
285 production of additional target molecules and thereby reduce the ratio of free antibiotic to target
286 molecules.

287

288 **Forecasting the resistance selection window**

289 Finally, we illustrate how COMBAT can be used to explore how the molecular mechanisms of
290 resistance mutations affect antibiotic concentrations at which resistance can emerge, i.e., the
291 resistance selection window. We compared predicted net growth rates as a function of
292 ciprofloxacin concentrations for a wild-type strain and an archetypal resistant strain. For this
293 analysis, we assumed that the resistant strain has a 100x slower drug-target binding rate (i.e.
294 ~100x increased MIC, realistic for novel point mutations[36]) and that the maximum replication
295 rate of the resistant strain is 85 % of the wild type strain[37]. We then predicted the antibiotic
296 concentrations at which resistance would be selected. Interestingly, when comparing COMBAT
297 to previous pharmacodynamics models (Fig. 5), we observed that estimates of replication rates
298 depend on the selected time frame (Fig. 6a). When the timeframe for MIC determination is set to
299 18 h as defined by CLSI[38], the "competitive resistance selection window", i.e., the
300 concentration range below the MIC of both strains where the resistant strain is fitter than the wild
301 type, ranges from 0.002 mg/L to 0.014 mg/L for ciprofloxacin (Fig. 6a) and 1 mg/L to 2.6 mg/L
302 for ampicillin (Supplementary Fig. S12), respectively. This corresponds well with previous
303 observations that ciprofloxacin resistance is selected for well below MIC[11]. However, when
304 measuring after 15 min or 45 min, the results are substantially different. The reason for this is
305 illustrated in Fig. 6b. COMBAT reproduces non-linear time kill curves where bacterial
306 replication continues until sufficient target is bound to result in a negative net growth rate. This
307 compares well with experimental data around MIC in Fig. 3a and 5a. In Fig. 6b, we show model
308 predictions for ciprofloxacin concentrations corresponding to a zero net growth (i.e. same
309 population size) after 15 min, 45 min and 18 h ($MIC_{Resistant;\ 15\ min}$, $MIC_{Resistant;\ 45\ min}$,

310 $MIC_{Resistant;\ 18\ h}$). In all cases, the bacterial population first increases and then decreases slowly.
311 This may have consequences for the selection of resistant strains. Fig. 6c illustrates how the
312 resistance selection windows depending on the observed time frame. This suggests that even at
313 concentrations above the 18 h MIC of the resistant strain, there may be initial growth of the
314 resistant strain. In this case, the resistant strain could continue growing at concentration of up to
315 7 mg/L ciprofloxacin at 15 min, even though the MIC at 18 h is 1.27 mg/L.
316
317 **Discussion**
318 Optimizing dosing levels of antibiotics is important for maximizing drug efficacy against wild-
319 type strains as well as for minimizing the rise of resistant mutants. The determination of optimal
320 dosing strategies typically requires expensive empirical studies; the need for such studies arises
321 in part from our currently limited capacity to predict how antibiotics will affect bacteria at a
322 given concentration. In fact, drug attrition is mainly due to insufficient predictions of efficacy
323 (pharmacodynamics) rather than pharmacokinetics[6]. For optimizing drug development and for
324 minimizing resistance, we need quantitative predictions for antibiotics or resistant bacterial
325 strains that do not exist yet. The ability to accurately predict MICs on the basis of biochemical
326 parameters and, more generally, to define antibacterial activity across a range of drug
327 concentrations, would allow us to estimate antibiotic efficacy for novel compounds or against not
328 yet emerged resistant strains[15, 39]. Recent studies have reported methods to predict MICs from
329 whole genome sequencing data[40, 41]. However, these methods require transfer of prior
330 knowledge on how the resistance mutations affect MICs in other organisms. There are no
331 methods that could predict *a priori* how chemical changes to an antibiotic structure or novel
332 resistance mutations affect bacterial growth at a given antibiotic concentration.
333

334 Here, we accurately predict antibiotic action on the basis of accessible biochemical parameters of
335 drug-target interaction. Our computational model, COMBAT provides a framework to predict
336 the efficacy of compounds based on drug-target affinity, target number, and target occupancy.
337 These parameters may change both when improving antibiotic lead structures as well as when
338 bacteria evolve resistance. Importantly, they can be measured early in drug development and
339 may even be a by-product of target-based drug discovery[42]. When these data are available,
340 COMBAT makes only one assumption: that the rate of bacterial replication decreases and/or the
341 rate of killing increases with successive target binding. While fitting, we allow this relationship
342 to be gradual or abrupt and select the best fit. This means we do not model specific molecular
343 mechanisms down-stream of drug-target binding, but their effects are subsumed in the functions
344 that connect the kinetic of drug-target binding to bacterial replication and death.
345
346 In previous work, for example on antipsychotics[16], antivirals[17] and antibiotics[15, 18],
347 models of drug-target binding kinetics have been used to improve our qualitative understanding
348 of pharmacodynamics. Our study substantially advances this work by making accurate
349 quantitative predictions across antibiotics and bacterial strains when measurable biochemical
350 characteristics change. This is possible because COMBAT employs an elegant mathematical
351 approach, based on partial differential equations, that makes it computationally feasible to fit the
352 model to a large range of data. Importantly, we are not only able to predict antibiotic action from
353 biochemical parameters, but can also vice versa use COMBAT to accurately predict biochemical
354 changes from observed patterns of antibiotic action. We have confirmed the excellent predictive
355 power of COMBAT with clinical data as well as experiments with antibiotics with very different
356 mechanisms of action. This gives us confidence that biochemical parameters are major

357 determinants of antibiotic action in bacteria and that COMBAT helps to make rational decisions
358 about antibiotic dosing.
359
360 In drug development, our mechanistic modeling approach provides insight into which chemical
361 characteristics of drugs may be useful targets for modification. For example, our sensitivity
362 analyses indicate that antibiotics with a similar affinity but faster binding inactivate bacteria
363 more quickly and therefore prevent replication and production of more target molecules, which
364 would change the ratio of antibiotic to target. Furthermore, because e.g. antibiotic binding and
365 unbinding rates can be determined early in the drug development process, such insight can help
366 the transition to preclinical and clinical dosing trials. This may contribute to reducing bottlenecks
367 between these phases of drug development and thereby save money and time.
368
369 Avoiding antibiotic concentrations that select for resistance is challenging because the precise
370 concentrations are only known after extensive experiments have been performed that identify the
371 MIC of (nearly) all possibly emerging resistant mutants. Predicting the resistance selection
372 windows of novel resistant mutants on the basis of biologically plausible changes in drug-target
373 binding would allow us to better assess what drug concentrations need to be achieved to avoid
374 selection of resistance. This approach offers new promise to assess resistance risks prior to
375 characterizing the majority of resistance mutations and thereby reduce the failure rates of
376 candidate compounds late in the drug development process when resistance is observed in
377 patients and substantial resources have been invested.
378

379 Our approach also offers insight into determinants of the resistance selection window. Rather
380 than determining the resistance selection window for a comprehensive collection of possibly
381 arising resistance mutations in each bacteria-drug pair, it would be attractive to build
382 transferrable knowledge that allows estimating the resistance selection window. In concordance
383 with a recent meta-analysis of experimental data[43], our sensitivity analyses predict that
384 changes in drug target binding and unbinding have a greater impact on the MIC than changes in
385 target molecule content or down-stream processes. Thus, a more comprehensive characterization
386 of the binding parameters of spontaneous resistant mutants would allow an overview of the
387 maximal biologically plausible levels of resistance that can arise with one mutation. Dosing
388 above this level should then safeguard against resistance. This is especially useful for compounds
389 for which it is difficult to saturate the mutational target for resistance, or for safeguarding against
390 resistance to newly introduced antibiotics for which we do not yet have a good overview of
391 resistance conferring mutations. If toxicity, solubility or other constraints do not allow dosing
392 above the MIC of expected resistant strains, COMBAT can predict the concentration range at
393 which resistance is less strongly selected. This could guide decisions on treating with low versus
394 high doses, which is currently controversially debated[7, 8]. Good quantitative estimates on the
395 dose-response relationship of new drugs would also help defining the therapeutic window, i.e.
396 the range of drug concentrations at which the drug is effective but not yet toxic.
397
398 Our quantitative work can help to identify optimal dosing strategies at constant antibiotic
399 concentrations for homogeneous bacterial populations. These measures are commonly used to
400 assess antibiotic efficacy. In addition, previous work has demonstrated that drug-target binding
401 models can qualitatively describe antibiotic efficacy over the fluctuating concentrations that

402 actually occur in patients[26, 44]. They can also explain complicated phenomena such as
403 biphasic kill curves, the post-antibiotic effect, or the inoculum effect[15, 18, 45] that often
404 complicate the clinical phase of drug development. COMBAT has similar characteristics that
405 allow capturing these complex phenomena. Therefore, employing COMBAT may be useful for
406 guiding drug development to maximize antibiotic efficacy and minimize *de novo* resistance
407 evolution.
408

409 **Methods**

410 ***Mathematical model***

411 COMBAT incorporates the binding and unbinding of antibiotics to their targets and describes
412 how target binding affects bacterial replication and death. This work extends the model
413 developed in[18]. COMBAT consists of a system of two mass balance equations: one PDE for
414 bacteria (describing replication and death as a function of both time and target binding) and one
415 ODE for antibiotic molecules (describing the concentrations as function of time).
416

417 In the most basic version of COMBAT, we ignored differences between extracellular and
418 intracellular antibiotic concentrations and only followed the total antibiotic concentration A,
419 assuming that the time needed for drug molecules to enter bacterial cells is negligible. We model
420 ciprofloxacin (to which there is a limited diffusion barrier[46]) and ampicillin (where the target
421 is not in the cytosol, even though the external membrane in gram negatives has to be crossed to
422 reach PBPs). We therefore believe that this assumption is justified in wild-type *E. coli*. This
423 basic version of COMBAT is therefore more accurate for describing antibiotic action where the
424 diffusion barrier to the target is weak.

Binding kinetics

We describe the action of antibiotics as a binding and unbinding process to bacterial target molecules[18]. For simplicity, we assume a constant number of available target molecules θ. The binding process is defined by the formula $A + T \rightleftharpoons x$, where the intracellular antibiotic molecules A react with target molecules T at a rate k_f and form an antibiotic-target molecule complex x, where values for x range between 0 and θ. If the reaction is reversible, the complex dissociates with a rate k_r.

In[18], the association and dissociation terms are described by the following terms

$$\frac{dB_i(t)}{dt} = \overbrace{\hat{k}_f A(t)\big((\theta - i + 1)B_{i-1}(t) - (\theta - i)B_i(t)\big)}^{Association\ term} - \overbrace{k_r\big(iB_i(t) - (i+1)B_{i+1}(t)\big)}^{Dissociation\ term};\ i\epsilon[0,\theta] \quad (6)$$

where $\hat{k}_f = \frac{k_f}{V_{tot} n_A}$, k_f is the association rate, V_{tot} is the volume in which the experiment is performed, n_A is Avogadro's number, k_r is the dissociation rate, B_i is the number of bacteria with i bound targets, and θ is the total number of targets. Green denotes the association term, while the dissociation term is in orange.

This approach requires the use of a large number of ordinary differential equations, $(\theta + 1)$ for the bacterial population and one for the antibiotic concentration. To generalize this approach, we assume that the variable of bound targets is a real number $x \in \mathcal{R}$. Under this continuity assumption, we consider the bacterial cells as a function of x and the time t, thereby reducing the total number of equations to two.

Under the continuity approximation $(x \in \mathcal{R})$, we can rewrite the binding kinetics in the form

$$\frac{\partial B(x,t)}{\partial t} = \overbrace{\frac{\partial}{\partial x}\left(\hat{k}_f A(t)(\theta - x)B(x,t)\right)}^{Association\ term} - \overbrace{\frac{\partial}{\partial x}\left(k_r x B(x,t)\right)}^{Dissociation\ term} \quad (7)$$

or simply

$$\frac{\partial B(x,t)}{\partial t} = \frac{\partial}{\partial x}\left(v_f(x,t)B(x,t) - v_r(x,t)B(x,t)\right) \quad (8)$$

where $v_f = \hat{k}_f A(t)(\theta - x)$ and $v_r = k_r x$ can be considered as two velocities, i.e., the derivative of the bound targets with respect to the time $\frac{dx}{dt}$. Green denotes the association term, while the dissociation term is in orange.

Replication rate

We assume that the replication rate of bacteria, $r(x)$, is dependent on the number of bound target molecules x. The function $r(x)$ is a monotonically decreasing function of x, such that fewer bacteria replicate as more target is bound. $r(0)$ is the maximum replication rate, corresponding to the replication rate of bacteria in absence of antibiotics. Thus, $r(x)$ describes the bacteriostatic action of the antibiotics, i.e., the effect of the antibiotic on bacterial replication.

Carrying capacity

Replication ceases as the total bacterial population approaches the carrying capacity K. At that point, the replication term of the equation is

$$\frac{\partial B(x,t)}{\partial t} = r(x)B(x,t)\frac{K - \int_0^\theta B(x,t)dx}{K} = r(x)B(x,t)F_{lim} \quad (9)$$

where $F_{lim} = \frac{K - \int_0^{\theta} B(x,t)dx}{K}$ is the replication-limiting term due to the carrying capacity K, and $0 \leq F_{lim} \leq 1$.

Distribution of target molecules upon division

We assume that the total number of target molecules doubles at replication, such that each daughter cell has the same number as the mother cell. We also assume that the total number of drug-target complexes is preserved in the replication and that the distribution of x bound target molecules of the mother cell to its progeny is described by a hypergeometric sampling of n molecules from x bound and $2\theta - x$ unbound molecules. Under the continuity assumption, we generalize the concept of hypergeometric distribution. Because the hypergeometric distribution is a function of combinations and because a combination is defined as function of factorials, we can use Γ functions in place of factorials and redefine a continuous hypergeometric distribution as a function of Γ functions. A Γ function is

$$\Gamma(\zeta) = \int_0^{\infty} x^{\zeta - 1} e^{-x} dx;\ Re(\zeta) > 0 \tag{10}$$

where ζ is a complex number. In this way, the distribution can be expressed as a probability density function of continuous variables. The amount of newborn bacteria is given by the term $r(x)B(x,t)F_{lim}(t)$. We assume that bound target molecules are distributed randomly between mother and daughter cells, with each of them inheriting 50% upon division on average. This means that twice the amount of newborn cells must be redistributed along x to account for the random distribution process. For example, if a mother cell with 4 bound targets divides, we have two daughter cells, each with a number of bound targets between 0 and 4 (their sum has to be 4), following the generalized hypergeometric distribution. For simplicity, we define $S(x,t)$ to be a

491 function related to the replication rate that depends on the number of bacteria with a number of
492 bound target molecules ranging between x and θ, their specific replication rate $r(x)$, and the
493 fraction of their daughter cells expected to inherit x antibiotic-target complexes $h(x,z)$:

494 $$S(x,t) = 2\int_x^\theta h(x,z)r(z)B(z,t)\,dz \quad (11)$$

495

496 *Death rate*

497 The death rate function $\delta(x)$ depends on the number of bound target molecules. The function
498 $\delta(x)$ is assumed to be a monotonically increasing function of x, where $\delta(\theta)$ is the maximum
499 death rate, when all targets in the bacteria have been bound by antibiotics. The shape of this
500 function describes the bactericidal action of the antibiotic.

501

502 *Bacteriostatic and bactericidal effects*

503 We consider several potential functional forms of the relationship between the percentage of
504 bound targets and replication and death rates, because the exact mechanisms how target
505 occupancy affects bacteria is unknown (Supplementary Fig. S1). We use a sigmoidal function
506 that can cover cases ranging from a linear relationship to a step function. When the inflection
507 point of a sigmoidal function is at 0 % or 100 % target occupancy, the relationship can also be
508 described by an exponential function. We assume that replication in bactericidal and death in
509 bacteriostatic drugs is independent of the amount of bound target. With sufficient experimental
510 data, the replication rate $r(x)$ and/or the death rate $\delta(x)$ can be obtained by fitting COMBAT to
511 time-kill curves of bacterial populations after antibiotic exposure. The sigmoidal shape of $r(x)$
512 and $\delta(x)$ can be written as:

513 $$r(x) = \frac{r_0}{1+e^{\gamma_r(x-x_{rth})}};\ \delta(x) = \frac{d_{max}}{1+e^{-\gamma_d(x-x_{dth})}} \quad (12)$$

where x_{rth} is the replication rate threshold, x_{dth} is the death rate threshold, and both represent the point where the sigmoidal function reaches ½ of its maximum. γ_r and γ_d represent the shape parameters of the replication and death rate functions, respectively. These factors determine the steepness around the inflection point. When they are extreme, the relationship approaches a linear or a step function.

Full equation describing bacterial population

Putting these components together, the full equation describing a bacterial population is:

$$\frac{\partial B(x,t)}{\partial t} + \overbrace{\frac{\partial}{\partial x}\left(v_f(x,t)B(x,t) - v_r(x,t)B(x,t)\right)}^{Binding\ kinetics} =$$

$$\overbrace{-r(x)B(x,t)F_{lim}(t) + S_B(x,t)F_{lim}(t)}^{Replication\ and\ its\ effects\ on\ binding} - \overbrace{\delta(x)B(x,t)}^{Death} \qquad (13)$$

where $B(x,t)$ is the number of bacteria. As in equations 2, 6, 7 and 8, green denotes the binding term, orange the unbinding term (together the binding kinetics is given in brown), blue the term describing bacterial replication and red the term describing bacterial death.

Equation describing antibiotic concentration

The free antibiotic concentration results from mass conservation, i.e., all antibiotic molecules associating with their target are subtracted and all dissociating antibiotic molecules are added. Equation 3 in the results section describes the dynamics of the antibiotic concentration.

Description of beta-lactam action

536 Beta-lactams acetylate their target molecules (PBPs) and thereby inhibit cell wall synthesis. The
537 acetylation of PBPs consumes beta-lactams. However, PBPs can recover through deacetylation.
538 We modified the term of drug-target dissociation in the equation describing antibiotic
539 concentrations (equation 3), and set the unbinding rate $k_r = 0$. To reflect the recovery of target
540 molecules, we substituted the dissociation rate k_r in the equation describing the bacterial
541 population with the deacetylation rate k_a, as described in[26].
542
543 *Initial and boundary conditions*
544 At $t = 0$, we assume that all bacteria have zero bound targets ($x = 0$), and the initial
545 concentration of bacteria is $B(x, 0) = 0, x > 0$, and $B(0,0) = B_0$.
546 At the boundaries of the partial differential equation ($x = 0, x = \theta$), we specify that the outgoing
547 velocities are zero. For $x = 0$, i.e. no bound target molecules, the unbinding velocity $v_r(0, t) =$
548 0, and in $x = \theta$, i.e. all targets are bound, the binding velocity $v_f(\theta, t) = 0$. When the
549 replication term at $x = 0$ and the death term at $x = \theta$ are known, we can solve the partial
550 differential equation with two ordinary differential equations at the boundaries. They are similar
551 to the equations at $x = 0$ and at $x = \theta$ described by Abel zur Wiesch et al.[18], but taking into
552 account that x is a continuous variable instead of a natural number.
553
554 *Numerical schemes*
555 To solve our system of differential equations, we used a first-order upwind scheme. Specifically,
556 we used the spatial approximation $u_-^f = \frac{u(i)-u(i-1)}{\Delta x}$ for the binding term ($v_f > 0$) and the spatial
557 approximation $u_+^f = \frac{u(i+1)-u(i)}{\Delta x}$ for the unbinding term ($v_r < 0$). For the time approximation of

558 both the PDEs and the ODEs, we used the forward approximation $\frac{\Delta B}{\Delta t} = \frac{B^{n+1} - B^n}{\Delta t}$[47]. We also

559 verified that the Courant-Friedrichs-Lewy condition is satisfied. For fitting the experimental data

560 of bacteria exposed to ciprofloxacin and ampicillin, we used the particle swarm method

561 ("particleswarm" function in Matlab, MathWorks software).

562

563 *Concentrations of gyrase A_2B_2 tetramers*

564 We assumed that gyrases A and B first homo-dimerize to A_2 and B_2, respectively, which in turn

565 bind to each other to form the tetramer TR[48]. The following system of equations describes

566 their binding kinetics:

567
$$\begin{cases} \frac{dA}{dt} = -2k_1A^2 + 2k_{-1}A_2 \\ \frac{dB}{dt} = -2k_2B^2 + 2k_{-2}B_2 \\ \frac{dA_2}{dx} = k_1A^2 - k_{-1}A_2 - k_3A_2B_2 + k_{-3}TR \\ \frac{dB_2}{dt} = k_2B^2 - k_{-2}B_2 - k_3A_2B_2 + k_{-3}TR \\ \frac{dTR}{dt} = k_3A_2B_2 - k_{-3}TR \end{cases} \quad (14)$$

568
$$\begin{cases} A + A \underset{k_{-1}}{\overset{k_1}{\rightleftharpoons}} A_2 \\ B + B \underset{k_{-2}}{\overset{k_2}{\rightleftharpoons}} B_2 \\ A_2 + B_2 \underset{k_{-3}}{\overset{k_3}{\rightleftharpoons}} TR \end{cases} \quad (15)$$

569

570 First, we calibrated the model to ensure that we obtain the correct number of gyrase A_2B_2

571 tetramers (~100) per wild type bacterial cell[49, 50]. This results in an average of each 206

572 gyrase A and B monomers. Because the association and dissociation rates of the dimers and

573 tetramers are unknown, we sampled 10^4 sets of six parameters in equation 14 ($k_{-3}, \dots k_3$) in a

574 Latin hypercube approach from a biologically plausible range where the association rates are

575 between 10^7 - 10^9 M^{-1} s^{-1} and the dissociation rates between 10^{-3} - 10^{-1} s^{-1} [33]. This results in 10^4

576 estimates for each of the six experimental replicates quantifying gyrase A and B (Fig. 4,

577 Supplementary Fig. S2, Supplementary Tab. S3).

578

579 ***Experimental methods***

580 *Strains, growth conditions and strain construction*

581 *Escherichia coli* strain BW25113[51] (SoA2740) was transformed with plasmids pCA24N-

582 SC101-gyrAB[32] and pCA24N-SC101-ΔP-YFP[32] using electroporation, resulting in strains

583 BW25113/pCA24N-SC101-gyrAB (SoA3329) and BW25113/pCA24N-SC101-ΔP-YFP

584 (SoA3330), respectively. pCA24N-SC101-gyrAB encodes the *E. coli gyrAB* genes under control

585 of the IPTG inducible LacZ promoter. pCA24N-SC101-ΔP-YFP encodes a promoterless copy of

586 YFP and was used as a control. Bacteria were grown at 30°C on either LB agar or in LB broth,

587 both supplemented with 10 µg/mL chloramphenicol (Cm) and 10 µM (mild induction) or 100

588 µM (strong induction) of isopropyl β-D-1-thiogalactopyranoside (IPTG) (43714 5X, VWR

589 Chemicals) when necessary.

590

591 *Time-kill curves*

592 Overnight cultures of BW25113 or SoA3329 and SoA3330 were diluted 1:1000 in pre-warmed

593 LB or LB-Cm and LB-Cm-IPTG, respectively, and grown with shaking to OD_{600} ~0.5. A 1:3

594 dilution series of ciprofloxacin was made and added to the cultures at indicated concentrations.

595 Additional cultures without antibiotics and with a very high concentration of ciprofloxacin

596 (2.187 mg/L) were used to determine the minimal and maximal kill rate, respectively. Samples

597 were taken immediately prior to addition of the antibiotic and in ~20 min intervals or after 45

598 min, respectively. Samples were washed once in phosphate buffered saline (PBS) before colony
599 forming units (CFUs) were determined for each sample by plating a 1:10 dilution series in PBS
600 on LB agar plates.
601
602 *GyrAB quantification*
603 To quantify the relative amount of GyrAB, samples of SoA3329 and SoA3330 were collected
604 after 45 min of drug treatment as described above. An equal number of cells corresponding to 1
605 mL culture at OD_{600} = 1 were harvested by centrifugation. Pelleted cells were lysed at room
606 temperature for 20 min using B-PER bacterial protein extraction reagent (90078, Thermo
607 Scientific) supplemented with 100 µg/mL lysozyme, 5 units/mL DNaseI (all part of B-PER™
608 with Enzymes Bacterial Protein Extraction Kit, 90078, Thermo Scientifc) and 100 µM/mL
609 PMSF (52332, Calbiochem). Samples were stored at -80°C until further use.
610 Samples were heated to 70°C for 10 min after addition of 1x Bolt sample reducing agent (B0009,
611 Life Technologies) and 1x fluorescent compatible sample buffer (LC2570, Invitrogen). Proteins
612 in whole-cell lysates were separated on 4-15 % Mini-Protean TGX Precast gels (456-1085, Bio-
613 Rad) and transferred to 0.2 µm Nitrocellulose membranes (1704158, Bio-Rad).
614 Membranes were blocked in Odyssey blocking buffer-TBS (927-50000, Li-Cor) for at least one
615 hour at room temperature. Primary antibodies raised against GyrA (Rabbit α-Gyrase A, PA005,
616 Inspiralis), GyrB (Rabbit α-Gyrase B , PB005, Inspiralis), and CRP (Mouse α-*E. coli* CRP,
617 664304, Nordic Biosite antibodies) were diluted 1:250, 1:250, and 1:2,000 in Odyssey blocking
618 buffer-TBS, respectively. The blocked membranes were incubated with the appropriate primary
619 antibodies overnight at 4°C, washed 4x for 15 min each in TBS-T solution (Tris buffered saline
620 supplemented with Tween20: 0.138 M sodium chloride, 0.0027 M potassium chloride, 0.1 %

621 Tween20, pH 8.0 at 25°C), and incubated for 2 h at room temperature with fluorescent labelled
622 secondary antibodies (1:10,000 of IRDye® 680RD Goat anti-Mouse IgG, P/N 925-68070, Li-
623 Cor and 1:5000 of IRDye® 800CW Goat anti-Rabbit IgG, P/N 925-32211, Li-Cor) in Odyssey
624 blocking buffer-TBS. Finally, the membranes were washed 4x for 15 min each in TBS-T
625 solution and imaged at 700 nm and 800 nm using a Li-Cor Odyssey Sa scanning system.
626 Band intensities were quantified from unmodified images using the record measurement tool of
627 Photoshop CS6, normalized to the CRP loading control after background subtraction, and
628 reported relative to SoA3330. For clarity, the "levels" tool of Photoshop CS6 was used to
629 enhance the contrast of shown Western blot images.
630

631 **Data Availability**

632 Computer code will be available at https://www.abel-zur-wiesch-lab.com/.
633

634 **References**
635

636 1. Boeree MJ, Diacon AH, Dawson R, Narunsky K, du Bois J, Venter A, et al. A dose-ranging
637 trial to optimize the dose of rifampin in the treatment of tuberculosis. Am J Respir Crit Care Med.
638 2015;191(9):1058-65. doi: 10.1164/rccm.201407-1264OC. PubMed PMID: 25654354.
639 2. Lan AJ, Colford JM, Colford JM, Jr. The impact of dosing frequency on the efficacy of 10-
640 day penicillin or amoxicillin therapy for streptococcal tonsillopharyngitis: A meta-analysis. Pediatrics.
641 2000;105(2):E19. PubMed PMID: 10654979.
642 3. Roord JJ, Wolf BH, Gossens MM, Kimpen JL. Prospective open randomized study
643 comparing efficacies and safeties of a 3-day course of azithromycin and a 10-day course of
644 erythromycin in children with community-acquired acute lower respiratory tract infections.
645 Antimicrob Agents Chemother. 1996;40(12):2765-8. PubMed PMID: 9124837; PubMed Central
646 PMCID: PMCPMC163618.
647 4. Van Deun A, Salim MA, Das AP, Bastian I, Portaels F. Results of a standardised regimen for
648 multidrug-resistant tuberculosis in Bangladesh. Int J Tuberc Lung Dis. 2004;8(5):560-7. PubMed
649 PMID: 15137531.
650 5. WHO. The shorter MDR-TB regimen.
651 http://wwwwhoint/tb/Short_MDR_regimen_factsheetpdf?ua=1. 2016.

652 6. Waring MJ, Arrowsmith J, Leach AR, Leeson PD, Mandrell S, Owen RM, et al. An analysis
653 of the attrition of drug candidates from four major pharmaceutical companies. Nat Rev Drug
654 Discov. 2015;14(7):475-86. Epub 2015/06/20. doi: 10.1038/nrd4609. PubMed PMID: 26091267.
655 7. Kouyos RD, Metcalf CJ, Birger R, Klein EY, Abel zur Wiesch P, Ankomah P, et al. The
656 path of least resistance: aggressive or moderate treatment? Proc Biol Sci. 2014;281(1794):20140566.
657 doi: 10.1098/rspb.2014.0566. PubMed PMID: 25253451; PubMed Central PMCID:
658 PMCPMC4211439.
659 8. Read AF, Day T, Huijben S. The evolution of drug resistance and the curious orthodoxy of
660 aggressive chemotherapy. Proc Natl Acad Sci U S A. 2011;108 Suppl 2:10871-7. doi:
661 10.1073/pnas.1100299108. PubMed PMID: 21690376; PubMed Central PMCID:
662 PMCPMC3131826.
663 9. Colijn C, Cohen T. How competition governs whether moderate or aggressive treatment
664 minimizes antibiotic resistance. Elife. 2015;4. doi: 10.7554/eLife.10559. PubMed PMID: 26393685;
665 PubMed Central PMCID: PMCPMC4641510.
666 10. Drlica K, Zhao X. Mutant selection window hypothesis updated. Clin Infect Dis.
667 2007;44(5):681-8. doi: 10.1086/511642. PubMed PMID: 17278059.
668 11. Gullberg E, Cao S, Berg OG, Ilback C, Sandegren L, Hughes D, et al. Selection of resistant
669 bacteria at very low antibiotic concentrations. PLoS Pathog. 2011;7(7):e1002158. doi:
670 10.1371/journal.ppat.1002158. PubMed PMID: 21811410; PubMed Central PMCID:
671 PMCPMC3141051.
672 12. Drlica K. The mutant selection window and antimicrobial resistance. J Antimicrob
673 Chemother. 2003;52(1):11-7. Epub 2003/06/14. doi: 10.1093/jac/dkg269. PubMed PMID:
674 12805267.
675 13. Sommer MOA, Munck C, Toft-Kehler RV, Andersson DI. Prediction of antibiotic
676 resistance: time for a new preclinical paradigm? Nat Rev Microbiol. 2017;15(11):689-96. Epub
677 2017/08/02. doi: 10.1038/nrmicro.2017.75. PubMed PMID: 28757648.
678 14. Muliaditan M, Davies GR, Simonsson USH, Gillespie SH, Della Pasqua O. The implications
679 of model-informed drug discovery and development for tuberculosis. Drug Discov Today.
680 2017;22(3):481-6. Epub 2016/10/26. doi: 10.1016/j.drudis.2016.09.004. PubMed PMID: 27693714.
681 15. Walkup GK, You Z, Ross PL, Allen EK, Daryaee F, Hale MR, et al. Translating slow-
682 binding inhibition kinetics into cellular and in vivo effects. Nat Chem Biol. 2015;11(6):416-23. Epub
683 2015/04/22. doi: 10.1038/nchembio.1796. PubMed PMID: 25894085; PubMed Central PMCID:
684 PMCPMC4536915.
685 16. Sykes DA, Moore H, Stott L, Holliday N, Javitch JA, Lane JR, et al. Extrapyramidal side
686 effects of antipsychotics are linked to their association kinetics at dopamine D2 receptors. Nat
687 Commun. 2017;8(1):763. Epub 2017/10/04. doi: 10.1038/s41467-017-00716-z. PubMed PMID:
688 28970469; PubMed Central PMCID: PMCPMC5624946.
689 17. Shen L, Rabi SA, Sedaghat AR, Shan L, Lai J, Xing S, et al. A critical subset model provides
690 a conceptual basis for the high antiviral activity of major HIV drugs. Sci Transl Med.
691 2011;3(91):91ra63. doi: 10.1126/scitranslmed.3002304. PubMed PMID: 21753122; PubMed Central
692 PMCID: PMCPMC3488347.
693 18. Abel zur Wiesch P, Abel S, Gkotzis S, Ocampo P, Engelstadter J, Hinkley T, et al. Classic
694 reaction kinetics can explain complex patterns of antibiotic action. Sci Transl Med. 2015;7(287). doi:
695 ARTN 287ra73
696 10.1126/scitranslmed.aaa8760. PubMed PMID: WOS:000354433900001.
697 19. Aldred KJ, Kerns RJ, Osheroff N. Mechanism of quinolone action and resistance.
698 Biochemistry. 2014;53(10):1565-74. Epub 2014/03/01. doi: 10.1021/bi5000564. PubMed PMID:
699 24576155; PubMed Central PMCID: PMCPMC3985860.

700 20. Shen LL, Pernet AG. Mechanism of inhibition of DNA gyrase by analogues of nalidixic acid:
701 the target of the drugs is DNA. Proc Natl Acad Sci U S A. 1985;82(2):307-11. PubMed PMID:
702 2982149; PubMed Central PMCID: PMCPMC397026.
703 21. Shen LL, Mitscher LA, Sharma PN, O'Donnell TJ, Chu DW, Cooper CS, et al. Mechanism
704 of inhibition of DNA gyrase by quinolone antibacterials: a cooperative drug--DNA binding model.
705 Biochemistry. 1989;28(9):3886-94. PubMed PMID: 2546585.
706 22. Andriole VT. <<The>> quinolones. 3rd ed. San Diego: Academic Press; 2000. XX, 517 S.
707 p.
708 23. Jungkind DL, American Society for Microbiology Eastern Pennsylvania Branch.
709 Antimicrobial resistance a crisis in health care. New York etc.: Plenum Press; 1995. X, 248 S. p.
710 24. Kampranis SC, Maxwell A. The DNA gyrase-quinolone complex. ATP hydrolysis and the
711 mechanism of DNA cleavage. J Biol Chem. 1998;273(35):22615-26. Epub 1998/08/26. PubMed
712 PMID: 9712890.
713 25. Siporin C, Heifetz CL, Domagala JM. The New generation of quinolones. New York: M.
714 Dekker; 1990. xii, 347 p., 2 p. of plates p.
715 26. Abel Zur Wiesch P, Clarelli F, Cohen T. Using Chemical Reaction Kinetics to Predict
716 Optimal Antibiotic Treatment Strategies. PLoS Comput Biol. 2017;13(1):e1005321. doi:
717 10.1371/journal.pcbi.1005321. PubMed PMID: 28060813; PubMed Central PMCID:
718 PMCPMC5257006.
719 27. Elliott TS, Shelton A, Greenwood D. The response of Escherichia coli to ciprofloxacin and
720 norfloxacin. J Med Microbiol. 1987;23(1):83-8. Epub 1987/02/01. doi: 10.1099/00222615-23-1-83.
721 PubMed PMID: 3546699.
722 28. Silva F, Lourenco O, Queiroz JA, Domingues FC. Bacteriostatic versus bactericidal activity
723 of ciprofloxacin in Escherichia coli assessed by flow cytometry using a novel far-red dye. J Antibiot
724 (Tokyo). 2011;64(4):321-5. Epub 2011/02/18. doi: 10.1038/ja.2011.5. PubMed PMID: 21326251.
725 29. Garoff L, Yadav K, Hughes D. Increased expression of Qnr is sufficient to confer clinical
726 resistance to ciprofloxacin in Escherichia coli. J Antimicrob Chemother. 2018;73(2):348-52. Epub
727 2017/11/07. doi: 10.1093/jac/dkx375. PubMed PMID: 29106520; PubMed Central PMCID:
728 PMCPMC5890660.
729 30. Sulavik MC, Houseweart C, Cramer C, Jiwani N, Murgolo N, Greene J, et al. Antibiotic
730 susceptibility profiles of Escherichia coli strains lacking multidrug efflux pump genes. Antimicrob
731 Agents Chemother. 2001;45(4):1126-36. Epub 2001/03/21. doi: 10.1128/AAC.45.4.1126-
732 1136.2001. PubMed PMID: 11257026; PubMed Central PMCID: PMCPMC90435.
733 31. Regoes RR, Wiuff C, Zappala RM, Garner KN, Baquero F, Levin BR. Pharmacodynamic
734 functions: a multiparameter approach to the design of antibiotic treatment regimens. Antimicrob
735 Agents Chemother. 2004;48(10):3670-6. doi: 10.1128/AAC.48.10.3670-3676.2004. PubMed PMID:
736 15388418; PubMed Central PMCID: PMCPMC521919.
737 32. Palmer AC, Kishony R. Opposing effects of target overexpression reveal drug mechanisms.
738 Nat Commun. 2014;5:4296. Epub 2014/07/02. doi: 10.1038/ncomms5296. PubMed PMID:
739 24980690; PubMed Central PMCID: PMCPMC4408919.
740 33. Fontana W. Lecture Notes: Continuous-Time Monte-Carlo of Reaction Systems.
741 34. Ocampo PS, Lazar V, Papp B, Arnoldini M, Abel zur Wiesch P, Busa-Fekete R, et al.
742 Antagonism between bacteriostatic and bactericidal antibiotics is prevalent. Antimicrob Agents
743 Chemother. 2014;58(8):4573-82. Epub 2014/05/29. doi: 10.1128/AAC.02463-14. PubMed PMID:
744 24867991; PubMed Central PMCID: PMCPMC4135978.
745 35. Chambers HF, Sachdeva MJ, Hackbarth CJ. Kinetics of penicillin binding to penicillin-
746 binding proteins of Staphylococcus aureus. Biochem J. 1994;301 (Pt 1):139-44. PubMed PMID:
747 8037661; PubMed Central PMCID: PMCPMC1137153.

748 36. Al-Emran HM, Heisig A, Dekker D, Adu-Sarkodie Y, Cruz Espinoza LM, Panzner U, et al.
749 Detection of a Novel gyrB Mutation Associated With Fluoroquinolone-Nonsusceptible Salmonella
750 enterica serovar Typhimurium Isolated From a Bloodstream Infection in Ghana. Clin Infect Dis.
751 2016;62 Suppl 1:S47-9. Epub 2016/03/05. doi: 10.1093/cid/civ790. PubMed PMID: 26933021.
752 37. Vogwill T, MacLean RC. The genetic basis of the fitness costs of antimicrobial resistance: a
753 meta-analysis approach. Evol Appl. 2015;8(3):284-95. Epub 2015/04/11. doi: 10.1111/eva.12202.
754 PubMed PMID: 25861386; PubMed Central PMCID: PMCPMC4380922.
755 38. Jorgensen JH, Ferraro MJ. Antimicrobial susceptibility testing: a review of general principles
756 and contemporary practices. Clin Infect Dis. 2009;49(11):1749-55. Epub 2009/10/28. doi:
757 10.1086/647952. PubMed PMID: 19857164.
758 39. Tonge PJ. Drug-Target Kinetics in Drug Discovery. ACS Chem Neurosci. 2018;9(1):29-39.
759 Epub 2017/06/24. doi: 10.1021/acschemneuro.7b00185. PubMed PMID: 28640596; PubMed
760 Central PMCID: PMCPMC5767540.
761 40. Metcalf BJ, Chochua S, Gertz RE, Jr., Li Z, Walker H, Tran T, et al. Using whole genome
762 sequencing to identify resistance determinants and predict antimicrobial resistance phenotypes for
763 year 2015 invasive pneumococcal disease isolates recovered in the United States. Clin Microbiol
764 Infect. 2016;22(12):1002 e1- e8. Epub 2016/08/21. doi: 10.1016/j.cmi.2016.08.001. PubMed PMID:
765 27542334.
766 41. Eyre DW, De Silva D, Cole K, Peters J, Cole MJ, Grad YH, et al. WGS to predict antibiotic
767 MICs for Neisseria gonorrhoeae. J Antimicrob Chemother. 2017;72(7):1937-47. Epub 2017/03/24.
768 doi: 10.1093/jac/dkx067. PubMed PMID: 28333355; PubMed Central PMCID: PMCPMC5890716.
769 42. Payne DJ, Gwynn MN, Holmes DJ, Pompliano DL. Drugs for bad bugs: confronting the
770 challenges of antibacterial discovery. Nat Rev Drug Discov. 2007;6(1):29-40. Epub 2006/12/13. doi:
771 10.1038/nrd2201. PubMed PMID: 17159923.
772 43. van der Putten BC, Pasquini G, Remondini D, Janes VA, Matamoros S, Schultsz C.
773 Quantifying the contribution of four resistance mechanisms to ciprofloxacin minimum inhibitory
774 concentration in Escherichia coli: a systematic review. 2018:372086. doi: 10.1101/372086 %J
775 bioRxiv.
776 44. Copeland RA. The drug-target residence time model: a 10-year retrospective. Nat Rev Drug
777 Discov. 2016;15(2):87-95. Epub 2015/12/19. doi: 10.1038/nrd.2015.18. PubMed PMID: 26678621.
778 45. Srimani JK, Huang S, Lopatkin AJ, You L. Drug detoxification dynamics explain the
779 postantibiotic effect. Mol Syst Biol. 2017;13(10):948. Epub 2017/10/25. doi:
780 10.15252/msb.20177723. PubMed PMID: 29061668; PubMed Central PMCID: PMCPMC5658699.
781 46. Cramariuc O, Rog T, Javanainen M, Monticelli L, Polishchuk AV, Vattulainen I. Mechanism
782 for translocation of fluoroquinolones across lipid membranes. Biochim Biophys Acta.
783 2012;1818(11):2563-71. Epub 2012/06/06. doi: 10.1016/j.bbamem.2012.05.027. PubMed PMID:
784 22664062.
785 47. Hirsch C. Numerical computation of internal and external flows : introduction to the
786 fundamentals of CFD. Oxford: Butterworth-Heinemann,; 2007. Available from:
787 http://app.knovel.com/web/toc.v/cid:kpNCIEFFC2.
788 48. Wu J, Zhang Z, Mitchenall LA, Maxwell A, Deng J, Zhang H, et al. The dimer state of GyrB
789 is an active form: implications for the initial complex assembly and processive strand passage.
790 Nucleic Acids Res. 2011;39(19):8488-502. Epub 2011/07/13. doi: 10.1093/nar/gkr553. PubMed
791 PMID: 21745817; PubMed Central PMCID: PMCPMC3201873.
792 49. Maier T, Schmidt A, Guell M, Kuhner S, Gavin AC, Aebersold R, et al. Quantification of
793 mRNA and protein and integration with protein turnover in a bacterium. Mol Syst Biol. 2011;7:511.
794 Epub 2011/07/21. doi: 10.1038/msb.2011.38. PubMed PMID: 21772259; PubMed Central
795 PMCID: PMCPMC3159969.

50. Malmstrom J, Beck M, Schmidt A, Lange V, Deutsch EW, Aebersold R. Proteome-wide cellular protein concentrations of the human pathogen Leptospira interrogans. Nature. 2009;460(7256):762-5. Epub 2009/07/17. doi: 10.1038/nature08184. PubMed PMID: 19606093; PubMed Central PMCID: PMCPMC2723184.
51. Datsenko KA, Wanner BL. One-step inactivation of chromosomal genes in Escherichia coli K-12 using PCR products. Proc Natl Acad Sci U S A. 2000;97(12):6640-5. Epub 2000/06/01. doi: 10.1073/pnas.120163297. PubMed PMID: 10829079; PubMed Central PMCID: PMCPMC18686.
52. Martinecz A, Abel Zur Wiesch P. Estimating treatment prolongation for persistent infections. Pathog Dis. 2018;76(6). Epub 2018/08/15. doi: 10.1093/femspd/fty065. PubMed PMID: 30107522; PubMed Central PMCID: PMCPMC6134427.

Acknowledgements

We thank Jingyi Liang, Vi Tran, Antal Martinecz, Giovanni Montani, Forrest W. Crawford, Roberto Natalini, Klaus Harms, Christoph Zimmer, Angelo Vannozzi and Rafal Mostowy for helpful discussions and feedback on the manuscript. We would like to acknowledge R. Regoes for providing previously published raw data. This work was funded by Bill and Melinda Gates Foundation Grant OPP1111658 (to T.C. & P.AzW.), Research Council of Norway (NFR) Grant 262686 (to P.AzW.) and 249979 (to S.A.), and Helse-Nord Grant 14796 (to S.A.).

Author Contributions

P.AzW. designed the study. F.C. developed the mathematical models. A.P., B.S., M.S., and S.A. designed the experiments. A.P., B.S., M.S., and S.L. performed the experiments. F.C., A.P., B.S., M.S., T.C., S.A., and P.AzW. analyzed the data. T.C., S.A., and P.AzW. wrote the manuscript.

Competing Interests statement

The authors declare no competing interests.

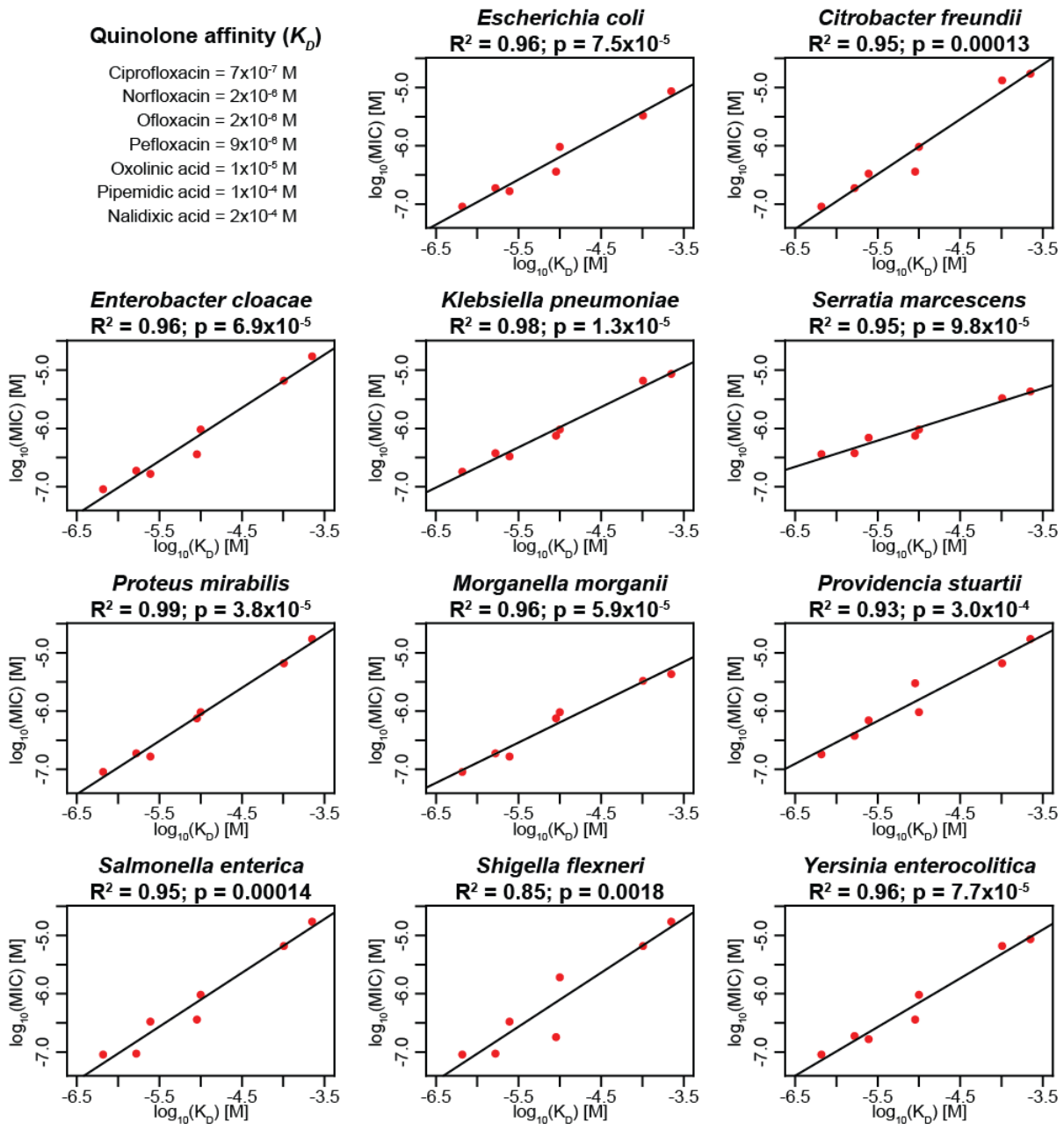

Fig. 1| Clinical data confirm linear correlation between MICs and affinities of quinolones to gyrase. We analyzed MIC and drug-target affinity data from 11 Enterobacteriaceae isolates and seven different quinolones. The x-axes show the affinities (K_D) as reported in the literature[21, 23-25], and the y-axes show the MICs, both in mol/L. The adjusted R^2 and p-value of each correlation are given. In cases where there was more than one K_D value reported in the literature,

829 we used the mean for this analysis. The tested MIC values are the median of several clinical

830 isolates described previously[25].

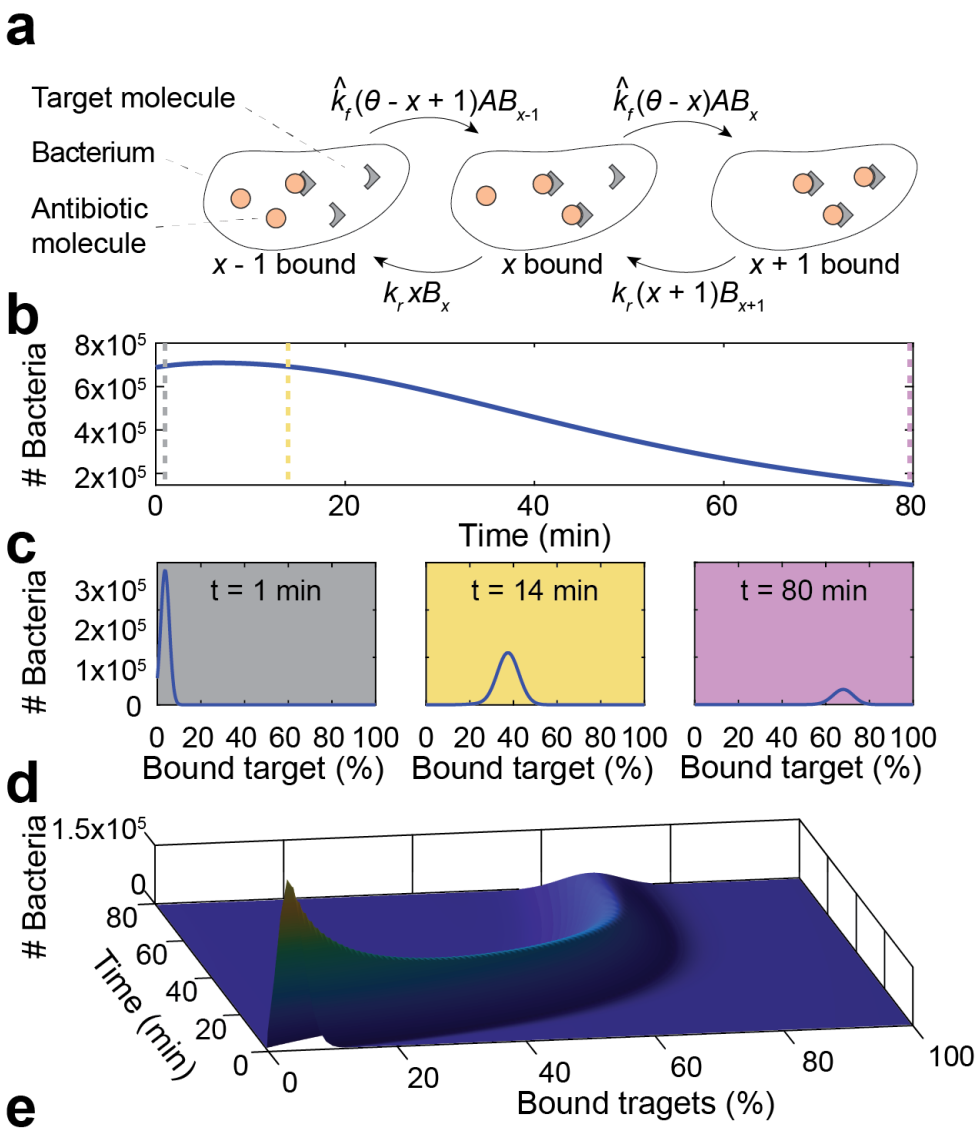

e

Parameters	Explanation	Functions	Explanation
k_f	Binding rate	$r(x)$	Growth rate
$\hat{k}_f = \frac{k_f}{n_A V_t}$	Binding rate rescaled to single molecules, n_A = Avogadro number, V_t = total volume of bacteria plus surrounding medium	$\delta(x)$	Death rate
		$S(x,t)$	Distribution of bound target molecules from mother to daughter cells
k_r	Unbinding rate		
K	Carrying capacity	$h(x,z)$	Generalized hyper-geometric function
θ	Targets per bacterium		

Fig. 2| Illustration of modeling approach. a, Schematic illustration of binding kinetics (adapted from[52]). The grey triangles depict the drug target molecules, and the orange circles represent antibiotic molecules within bacteria. The arrows indicate individual binding and unbinding events of the antibiotic to its target molecule in the cell. $\hat{k}_f$ is the adjusted forward reaction rate,

836 k_r is the reverse reaction rate, A is the concentration of antibiotics inside the bacterium, x is the
837 number of bound targets, θ is the number of targets and B_x is the number of bacteria with x bound
838 targets. **b**, Modeled sample time-kill curve, in which the sum of bacteria in all binding states (i.e.,
839 the entire population of living bacteria) is followed over time after exposure to antibiotics. The
840 vertical dotted lines indicate the time points depicted in (**c**); 1 min (grey), 14 min (yellow), and
841 80 min (purple). **c**, The percentage of bound antibiotic targets in the bacterial population at
842 indicated time points. **d**, Illustration of how the partial differential equation describes the
843 bacterial population as a surface in a three-dimensional coordinate system, the dimensions of
844 which represent percent bound target (x-axis), time (y-axis), and number of bacteria (z-axis). The
845 three time points shown in (**c**) represent two-dimensional cross-sections at different points of the
846 y-axis. **e**, Overview of used parameters and functions.

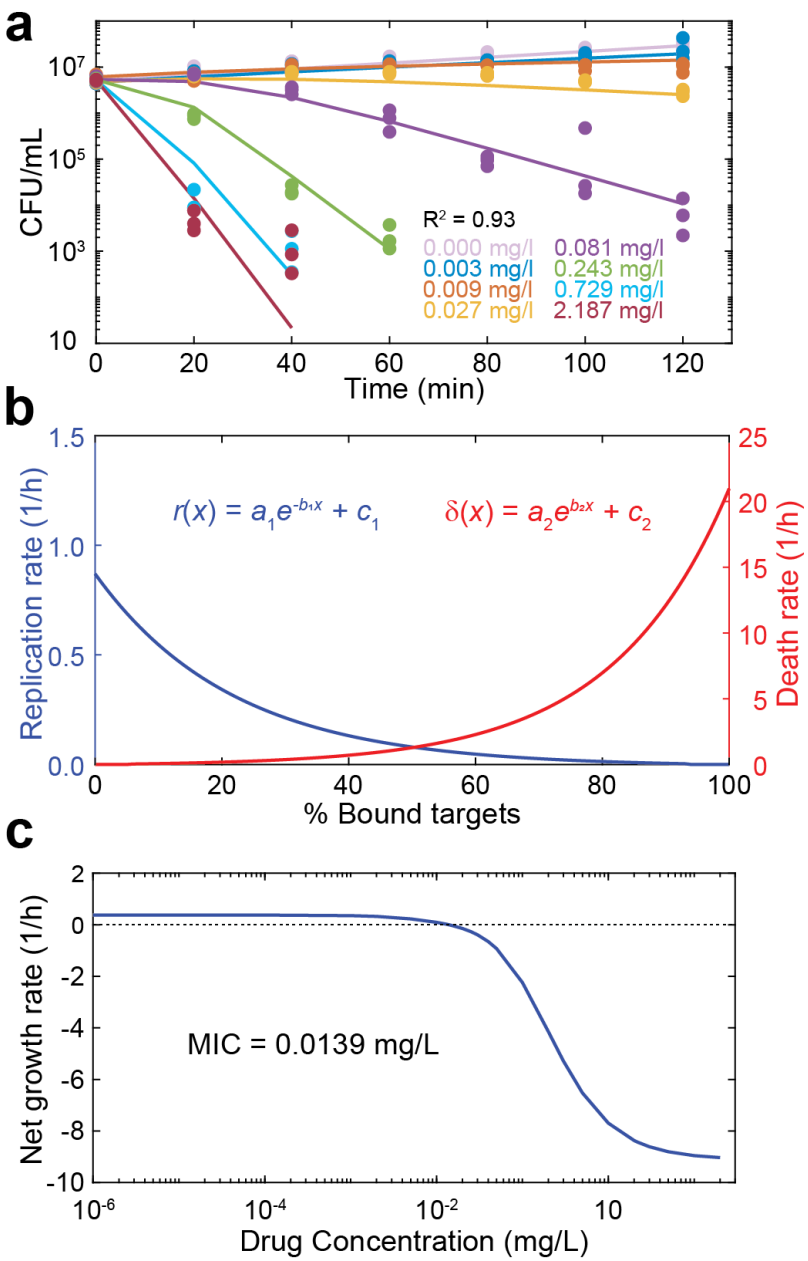

847

848 **Fig. 3| Model predictions for the MIC and the bacteriostatic and bactericidal effects of**

849 **ciprofloxacin. a**, Model fit to experimental time-kill curves. The points indicate the

850 experimental data of three independent replicates, and the lines indicate the model fit. Each color

851 indicates a ciprofloxacin concentration as reported in the figure. **b**, The blue line indicates the

852 bacteriostatic effect ($r(x)$, replication rate) of ciprofloxacin and the red line the bactericidal effect

853 ($\delta(x)$, death rate) as a function of the number of bound targets predicted by the model fit in (**a**).

854 The values of the fitted parameters are listed in Supplementary Tab. S2. **c**, The net growth rate as
855 determined by the slope of a line connecting the initial bacterial density and the final bacterial
856 density of a time-kill curve at 18 h on a logarithmic scale, is given as function of the drug
857 concentration (blue). The dotted horizontal line indicates zero net growth, and the intersection
858 with the blue line predicts the MIC (0.0139 mg/mL).

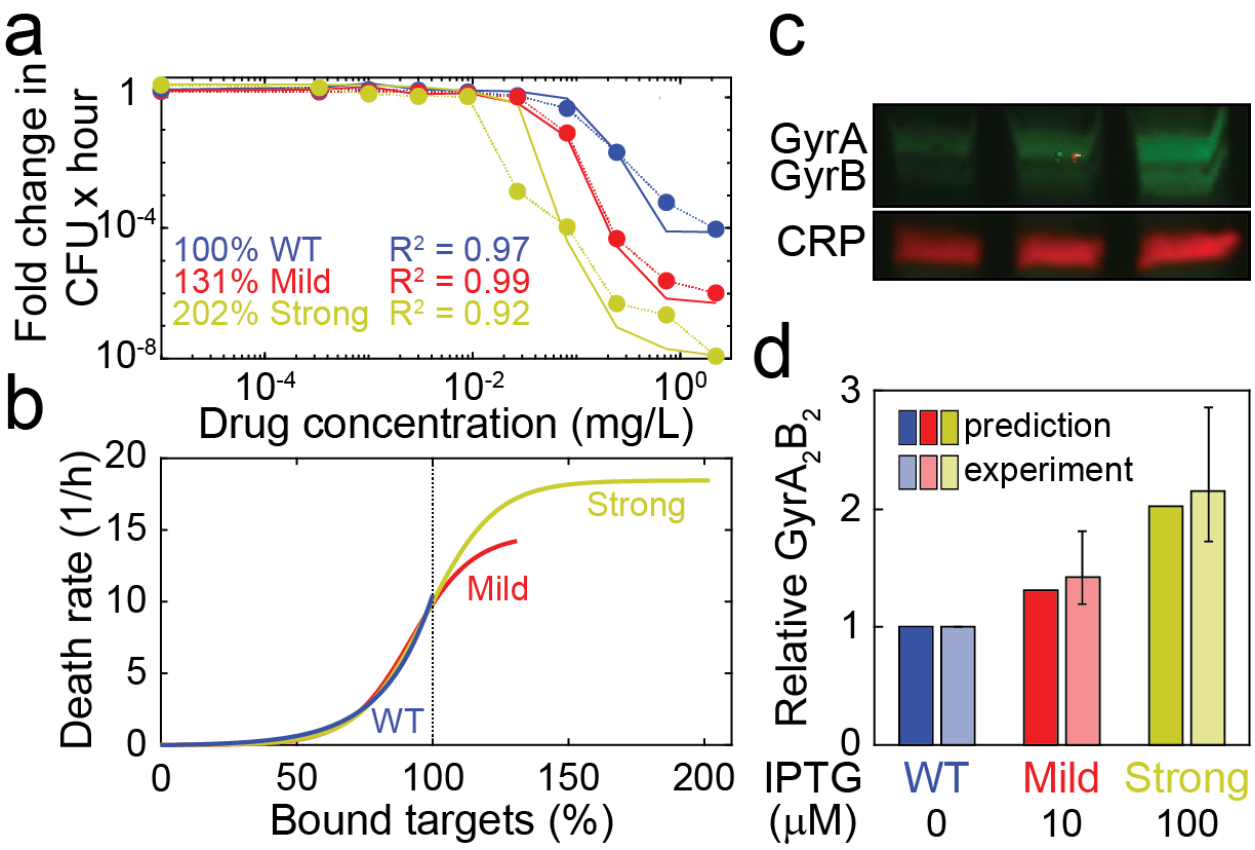

Fig. 4| Prediction of relative antibiotic target molecule content from time-kill curves. a, Dose-response curves of *E. coli* expressing *gyrA* and *gyrB* under the same IPTG-inducible promoter (SoA3329) grown in the presence of 10 μM IPTG (mild overexpression; red) and 100 μM IPTG (strong overexpression; yellow). A control strain (SoA3330), which expresses wild-type GyrAB levels and contains a mock plasmid, is grown in the absence of inducer (blue). The x-axis indicates the ciprofloxacin concentration, and the y-axis indicates the fold change in colony forming units over time. The dotted lines indicate experimental data, and the solid lines indicate the model fit. The best model fit was obtained for relative target molecule contents of 131 % (mild overexpression) and 202 % (strong overexpression) relative to the control strain (WT). **b**, Death rates of *E. coli* expressing different levels of GyrAB. The colors represent GyrAB expression conditions as in (**a**). The x-axis shows the percentage of bound antibiotic

871 target normalized to the control strain; the y-axis shows the death rate δ(x). Each line represents
872 the best fit for δ(x). **c**, Western blot analysis of GyrA&B in the strains/conditions shown in (**a**).
873 CRP (cAMP receptor protein) was used as loading control. A representative example of six
874 replicates is shown; see Supplementary Fig. S2 for full blots. **d**, comparison of theoretical
875 prediction (from (**b**), solid colors) and $GyrA_2B_2$ tetramer levels estimated from relative GyrA&B
876 monomer levels (quantified in (**c**), translucent colors). For the experimental measurements, the
877 bars indicate the mean, and the whiskers represent the 95 % confidence interval.

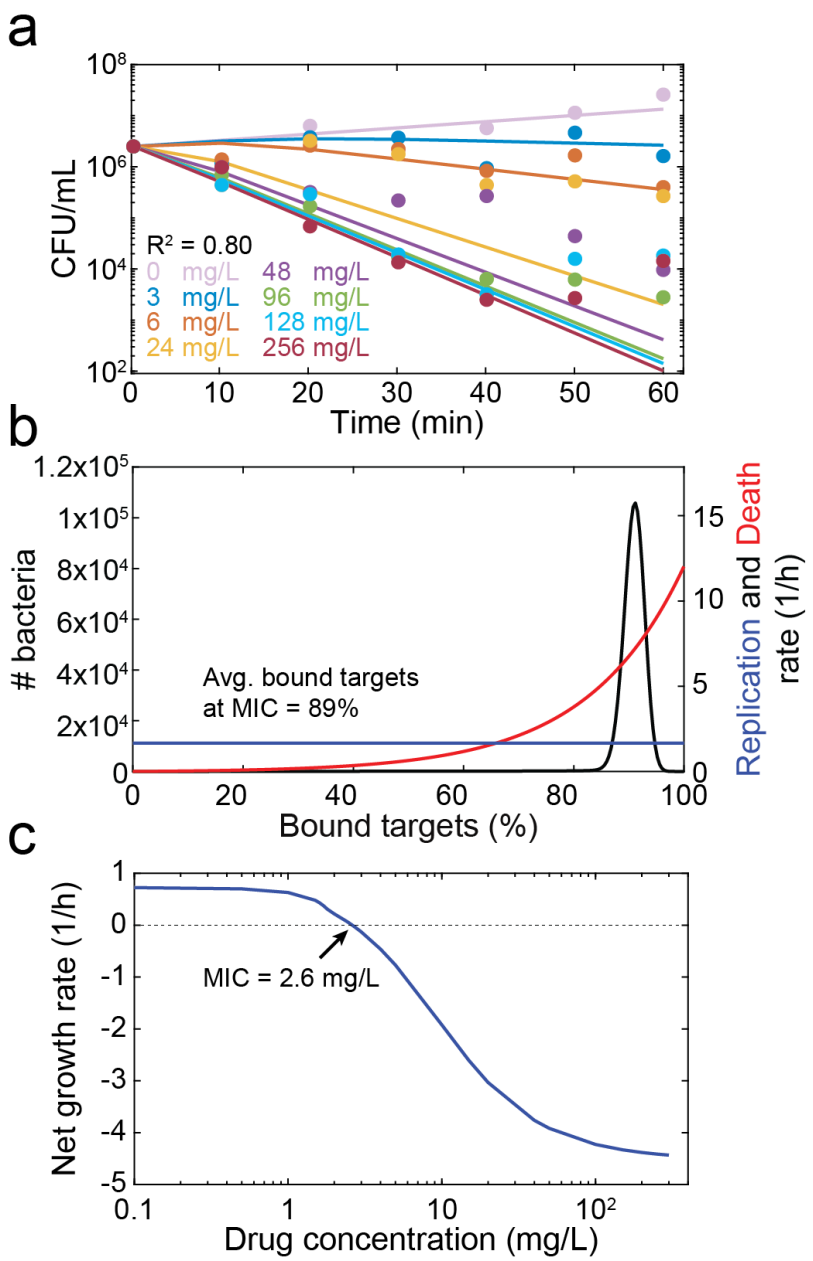

878

879 **Fig. 5| Model prediction of MIC and target occupancy at MIC for ampicillin. a**, Model fit to

880 previously published time-kill curves[31]. The points represent experimental data, and the lines

881 represent the fit of the model. Each color indicates a single ampicillin concentration, as described

882 in the legend. **b**, Replication (blue) and death (red) rates as a function of the number of bound

883 targets predicted by the model fit in (**a**). The black line indicates the predicted distribution of

884 target occupancies in a bacterial population (both living and dead cells) exposed to ampicillin at

885 the MIC for 18 h. **c**, The net growth rate, as determined by the slope of a line connecting the
886 initial bacterial density and the bacterial density at 18 h on a logarithmic scale predicted from the
887 model fit in (**a**), is shown as function of the drug concentration (blue). The dotted horizontal line
888 indicates zero net growth, and the intersection with the blue line predicts the MIC (2.6 mg/mL).

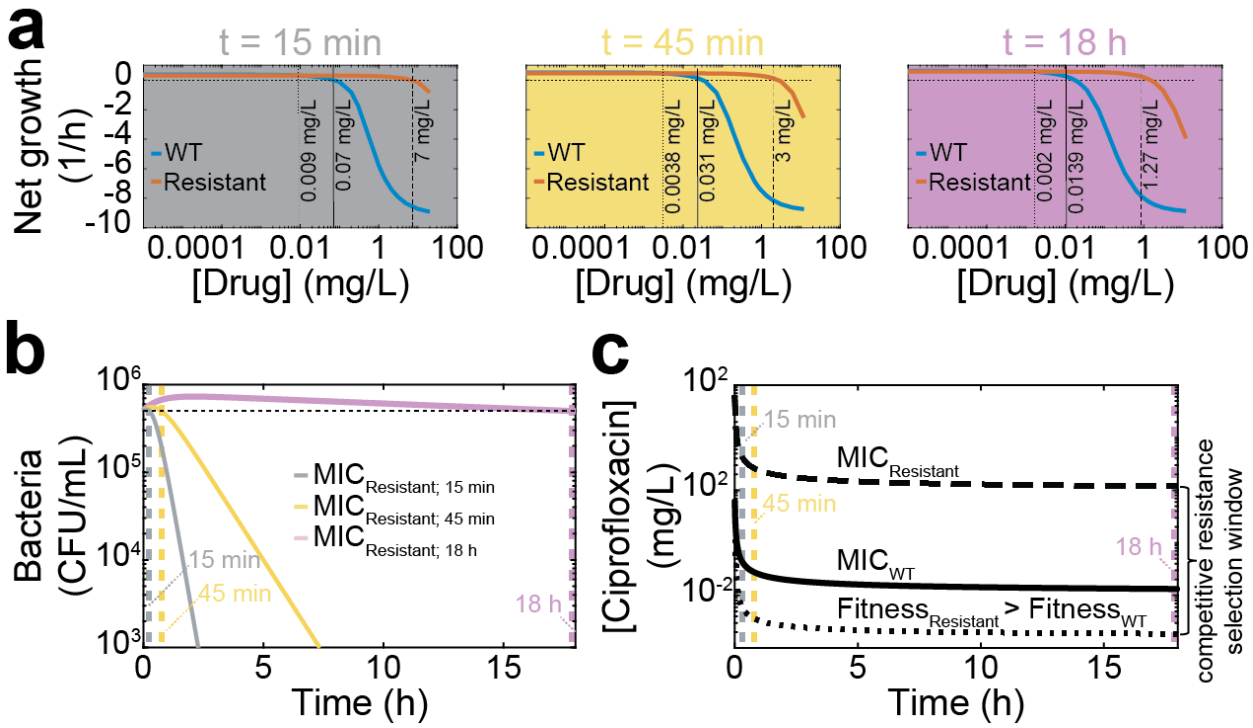

Fig. 6| Predicted mutation selection windows for *E. coli* exposed to ciprofloxacin. a, The drug concentration of ciprofloxacin is shown on the x-axes, and the average bacterial net growth rate in the first 15 min (grey panel), 45 min (yellow panel), and 18 h (purple panel) of exposure is given on the y-axes. The blue line represents the wild-type strain based on the fits shown in Fig. 3, and the red line represents a strain with a hypothetical resistance mutation that decreases the binding rate (k_f) 100-fold and imparts a 15 % fitness cost. The horizontal dotted line indicates no net growth. The vertical dotted line indicates where the resistant strain becomes more fit than the wild-type, the solid vertical line indicates the MIC of the wild-type, and the dashed vertical line indicates the MIC of the resistant strain. **b**, Modeled time kill curves of the resistant strain for ciprofloxacin concentrations at which there is no growth at 15 min (grey; $MIC_{15\ min}$ = 7 mg/L), 45 min (yellow; $MIC_{45\ min}$ = 3 mg/L) and 18 h (purple; $MIC_{18\ h}$ = 1.27 mg/L). The horizontal dotted line indicates the initial population size; the vertical dotted lines represent the time points at which the initial and final population size is the same. **c**, The mutation selection

903 window depends on the time at which bacterial growth is observed. The x-axis shows the
904 observed time at which replication rates were determined, the y-axis shows ciprofloxacin
905 concentrations. The dotted curve shows the ciprofloxacin concentration at which the resistant
906 becomes fitter than the WT ($Fitness_{Resistant} > Fitness_{WT}$), the solid line the MIC of the WT
907 (MIC_{WT}), and the dashed line the MIC of the resistant strain ($MIC_{Resistant}$). The area between the
908 dotted and dashed line indicates the competitive resistance selection window.